Binary pseudorandom array test standard optimized for characterization of large field-of-view optical interferometers

Valeriy V. Yashchuk, [*,a] Sergey Babin,[b] Stefano Cabrini,[c] Weilun Chao,[d] Ulf Griesmann,[e] Ian Lacey,[a] Stefano Marchesini,[f] Keiko Munechika,[g] Carlos Pina-Hernandez,[g] and Allen Roginsky[h]

[a]Advanced Light Source, Lawrence Berkeley National Laboratory, Berkeley, California 94720, USA; [b]aBeam Technologies, Inc., Hayward, California 94541, USA; [c]Molecular Foundry, Lawrence Berkeley National Laboratory, Berkeley, California, 94720, USA; [d]Materials Sciences Division, Lawrence Berkeley National Laboratory, Berkeley, California, 94720, USA; [e]Sensor Science Division, National Institute of Standards & Technology, Gaithersburg, Maryland 20899, USA; [f]Computational Research Division, Lawrence Berkeley National Laboratory, Berkeley, California 94720, USA; [g]HighRI Optics, Inc., 5401 Broadway Terr, St. 304, Oakland, California 94618, USA; [h]Computer Security Division, National Institute of Standards & Technology, Gaithersburg, Maryland 20899, USA

ABSTRACT

Recently, a technique for calibrating the modulation transfer function (MTF) of a broad variety of metrology instrumentation has been demonstrated. This technique is based on test samples structured as one-dimensional binary pseudo-random (BPR) sequences and two-dimensional BPR arrays (BPRAs). The inherent power spectral density of BPR gratings (sequences) and arrays has a deterministic white-noise-like character that allows direct determination of the MTF with uniform sensitivity over the entire spatial frequency range and field-of-view of an instrument. As such, the BPR samples satisfy the characteristics of a test standard: functionality, ease of specification and fabrication, reproducibility, and low sensitivity to manufacturing error. Here we discuss our recent developments directed to the optimization of the sample design, fabrication, application, and data processing procedures, suitable for thorough characterization of large aperture optical interferometers. Compared with the previous coded-aperture based design, the improved, 'highly randomized' BPRA pattern of the new test standard provides better accuracy and reliability of instrument MTF and aberration characterization, and enables operation optimization of large aperture optical interferometers. We describe the pattern generation algorithm and tests to verify the compliance to desired BPRA topography. The data acquisition and analysis procedures for different applications of the technique are also discussed.

Keywords: calibration, modulation transfer function, power spectral density, Fizeau interferometers, binary pseudorandom, test standard, aberration, surface metrology

1. INTRODUCTION

For a number of years, with the support of Department of Energy (DOE) Small Business Innovation Research (SBIR) grants, and using the capabilities of the Lawrence Berkeley National Laboratory (LBNL) Molecular Foundry [1] and Advanced Light Source (ALS) X-Ray Optics Laboratory (XROL) [2], we have been working on the development and commercialization of a technique for calibration of the Modulation Transfer Function (MTF) of a broad variety of metrology instrumentation (see, for example, Refs. [3,4] and references therein). The technique, recognized in 2015 with the R&D 100 Award, is based on test samples structured according to one-dimensional (1D) binary pseudo-random (BPR) sequences and two-dimensional (2D) BPR arrays (BPRAs).

Most of the BPRA samples we have developed for the characterization of 2D optical surface profilers, such as optical interferometric microscopes and Fizeau interferometers [3,4], were built according to the prescription for uniformly redundant arrays (URA) [5,6]. An example is shown in Fig. 1a. The inherent power spectral density (PSD) of such

* vvyashchuk@lbl.gov; phone 1 510 495-2592; fax 1 510 486-7696; lbl.gov

BPRA samples has a deterministic white-noise-like character that allows a direct determination of the MTF with a uniform sensitivity over the entire spatial frequency range and field-of-view of an instrument.

As such, the BPRA samples satisfy essential requirements of a test standard: functionality, ease of specification and fabrication, reproducibility, and low sensitivity to manufacturing error. This is in contrast to most of the common test patterns used in MTF measurements, including knife-edge sources (step height standards) [7–11], bar targets [12], sinusoidal [13] and periodical patterns [14,15], which do not meet these requirements.

However, as we have shown in our recent publication [4], the BPRAs, based on the URA prescription, have a limitation when used for the MTF calibration of surface profilers. This limitation is caused by the increased lower spatial frequency autocorrelation of a cropped URA pattern. The autocorrelation leads to an excess variation of the PSD distribution of the subareas of the URA BPRA sample shortened (cropped) in the course of the measurements. Subsequently, the accuracy of the MTF calibration decreases. The problem can be mitigated in measurements with the BPRA sample rotated by approximately 45° with respect to the pixel grid of the profiler's detector [4], but it is not possible to eliminate the effect.

While for the best performing MTF calibration, the inherent PSD of the cropped BPRA sample area, corresponding to the instrument's field-of-view, should have a white-noise-like character with minimum variation, for some other applications, the URA-based BPRA test samples are more preferable. For example, the URA pattern facilitates the measurements of the instrumental geometrical distortion. This is exploited in the data processing software pSpectra developed in the scope of the DOE Small Business Technology Transfer (STTR) project on MTF calibration of metrology profilometers that is also a part of the project.

The major goal of our work last year on the project was to develop 2D BPRA samples that have isotropic 2D PSDs (as illustrated in Fig. 1b) with minimal possible variation evaluated over different subareas of the total array when cropped by a factor of 2 to 3. Cropped subarrays are encountered in MTF measurements when the instrumental field-of-view is smaller than the total area of the BPRA test pattern. We call highly-randomized BPRA patterns with PSDs unaffected by cropping optimal BPRA patterns. Here, we report the major results of this work.

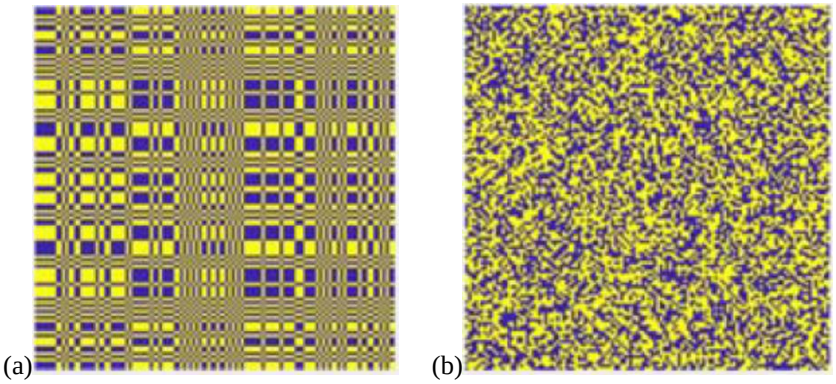

Figure 1. Binary pseudo-random arrays designed based on (a) the prescription for uniformly redundant arrays and (b) an optimal BPRA pattern, analogous to the one developed in the present work.

2. GENERATION OF A BPRA OPTIMAL FOR THE 2D MTF CALIBRATION

We have developed and tested an original algorithm for the generation of the 2D MTF-optimal arrays of randomly distributed 0's and 1's.

As the starting point, we use the pseudo-random number generator (pseudo-RNG) built in the Mathematica software. This pseudo-RNG, based on the "Extended CA" algorithm [16]. The algorithm is free of the sequence length limitation.

With the Mathematica pseudo-RNG, a list of random bits is generated that exceeds the length required for a 2D array with dimensions N_X and N_Y by a factor of about 10. This long random bit list is parsed into rows of length equal to the desired X pixel dimension, N_X. Sub regions are sequentially determined by joining a consecutive number of rows equal to the Y pixel dimension, N_Y. Each sub-region is summed and if the sub-region satisfies the condition of exactly 50 % duty cycle (the same number of 0's and 1's), the sub-region is considered a candidate for the 2D array, pending PSD analysis. If not, it is discarded and a new sub-region, shifted by one row, is tested.

The requirement for 50 % duty cycle is the distinguishing feature of our procedure for generating 2D BPRAs. It is helpful to minimize the variation of the mean value of the BPRA subareas and to design a highly-randomized array. The bias in the number of 0's and 1's across the entire array and its subareas can affect accuracy of the MTF calibration. The correlation between the random bits associated with the bias leads to low spatial frequency variation of the inherent PSD spectra. By requiring zero value of the bias factor, we design an array with higher randomization and with minimum variation of the PSD, inherent to the array subareas. Additionally, 50 % duty cycle corresponds to the maximum of the signal-to-noise ratio in the MTF measurements.

A total of twelve highly randomized 2D BPRAs with pixel dimensions of 4126 × 4126 and 50 % duty cycle were generated and tested. In Sec. 3, we briefly discuss the established mathematical criteria and corresponding procedures we use for selection of the BPRA pattern optimal for the MTF calibration of 2D surface profilers.

3. SELECTION OF A BPRA PATTERN OPTIMAL FOR CALIBRATION OF 2D MTF

At a glance, all 12 BPRAs generated look very similar. For better understanding of a suitability of an array as a pattern of a test sample for 2D MTF calibration, let us summarize the specific requirements to such a sample.

First, for the best performing calibration, the inherent PSDs of the MTF-optimal BPRA and its sub-arrays, corresponding to the instrument's field-of-view, should have white-noise-like character with minimum variation over the specified spatial frequency range, limited at the lower spatial frequencies by the total size of the array, and at the higher spatial frequencies by the elementary size of the BPRA pattern (that is the size of the smallest feature).

Second, the MTF-optimal BPRA and its sub-arrays should be isotropic (or rotation- and shift- symmetrical) in the sense that the PSDs of the array and its sub-arrays should not depend on the angular orientation of the array and its subarrays with respect to the detector grid.

Mathematically, both criteria are based on PSD analyzes of the generated arrays and its sub-areas.

A natural drawback of the BPRA generation procedure based on 'folding' of the long 1D random sequence is the possible asymmetry in randomness in two directions, along the rows and along the columns. Therefore, we specially check if the distribution of the PSD variations is random (white noise like) by using a statistical software EViews8 [17], used at the XROL also for stochastical modeling of the results of surface slope metrology with x-ray mirrors (see Refs [18] and references therein). Figure 2 illustrates the application of a standard histogram and statistics test of the EViews8 software to one of twelve BPRA generated with the Mathematica pseudo-RBG [16].

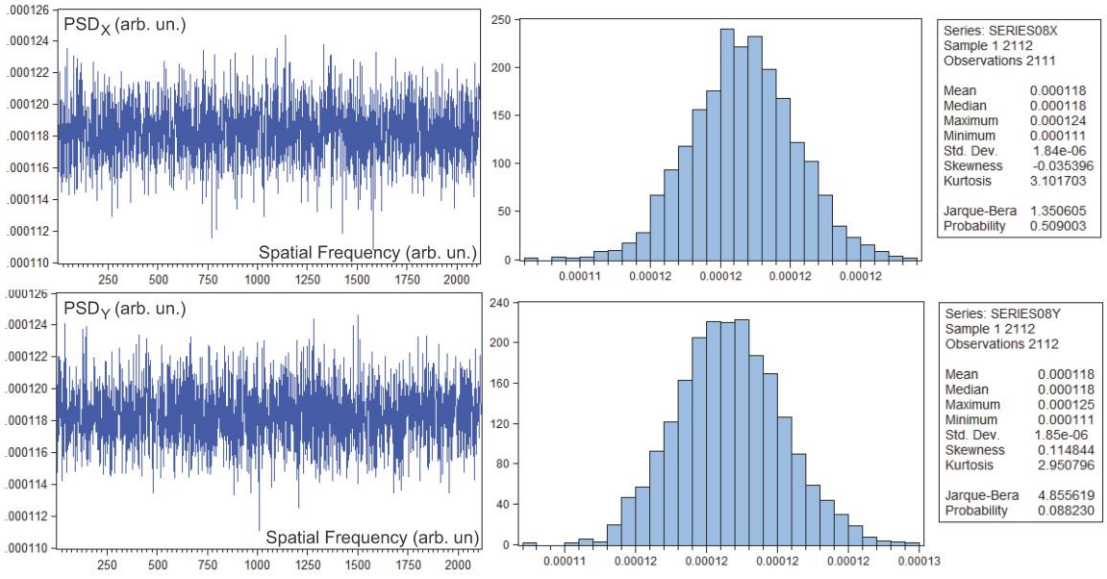

Figure 2. 1D PSD spectra and histograms of the residual PSD variations (after subtraction of the corresponding mean value) in the horizontal (the upper plots) and in the vertical (the bottom plots) directions. The tables present the results of verification of the null hypothesis of a normal distribution for the PSD_X and PSD_Y.

Next, we perform similar tests of the two-dimensional PSD spectra of the entire areas and different subareas of the twelve BPRAs, assuming that the MTF calibration with such test sample will be performed over such subareas, semi-randomly selected by the operator.

Among the 12 BPRAs, we select those with the smallest root-mean-square (RMS) variation of the 2D PSD spectrum around the constant level.

Note that the true RNGs based on physical processes (for example, photonic [19], quantum [20], and chaotic-laser-system [21] RNGs) are capable of providing true randomness, but the raw output of a physical source is typically biased and not uniformly distributed due to the nature of the physical processes. Therefore, additional algorithms are usually used to fix the problems and this complicates the entire generation procedure.

4. OPTIMAL BPRA TEST SAMPLES FOR THE 2D MTF CALIBRATION OF SURFACE PROFILERS

Based on the best highly randomized (optimal) BPRA pattern selected in the previous step, we have created the design files for nano-fabrication of optimal BPRA samples with elementary sizes between 300 nm and 2 μm, suitable for MTF characterization of optical microscopes. For larger field-of-view metrology tools, such as Fizeau interferometers, a photomask of a BPRA pattern with elementary size of 15 μm has been designed and fabricated (see also Sec. 5). Using the advanced micro- and nano-lithography capabilities of the LBNL Molecular Foundry [1], we have fabricated the desired optimal BPRA samples. The details of the fabrication process can be found in Ref. [4].

Figure 3 shows the highly-randomized BPRA samples patterned on super-polished silicon substrates with 2-in and 4-in diameters designed for the MTF characterization of optical microscopes (Fig. 3a) and large field-of-view Fizeau interferometers (Fig. 3b), respectively.

The new samples were tested in the MTF calibration experiments with two Fizeau interferometers and an interferometric microscope available at the LBNL ALS XROL [2].

Below in Secs. 5 and 6, we illustrate the advantages and new capabilities of the optimal BPRA test samples with 15-μm pixel size to characterize a 150-mm-diameter aperture Fizeau interferometer in two modes of operation of the laser light source: the ‘Spot’ mode with high spatial coherence, and the ‘Ring’ mode with low spatial coherence [22].

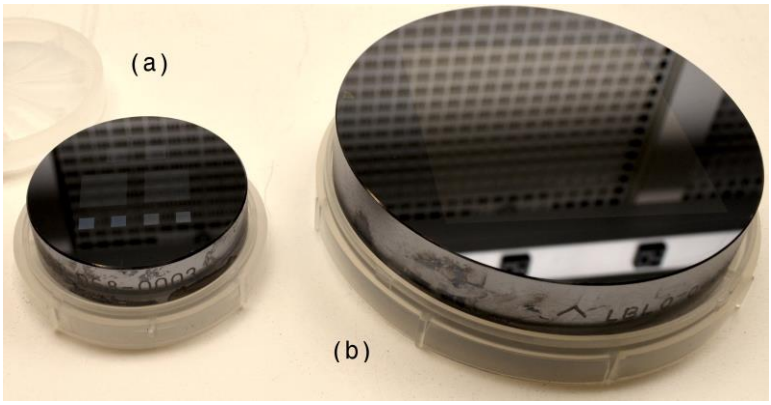

Figure 3. BPRA test samples developed for the MTF characterization of (a) optical microscopes and (b) large field-of-view Fizeau interferometers. The BPRA sample for the microscopes consists of a number of optimal BPRA patterns and BPRA patterns, based on the prescription for uniformly redundant arrays; both types of the BPRAs with different elementary size from 400 nm to 2 μm. This allows the characterization of the microscope in different arrangements of objectives and zooms.

5. 15-μm HIGHLY-RANDOMIZED BPRA SAMPLE OPTIMAL FOR CHARACTERIZATION OF A FIZEAU INTERFEROMETER

Figure 4 illustrates the major advantage of the highly-randomized BPRA sample, generated and selected as discussed above in Secs. 3 and 4, compared to the URA-based sample (Fig. 5) in the application to the spatial resolution (MTF) characterization of a commercial Fizeau interferometer.

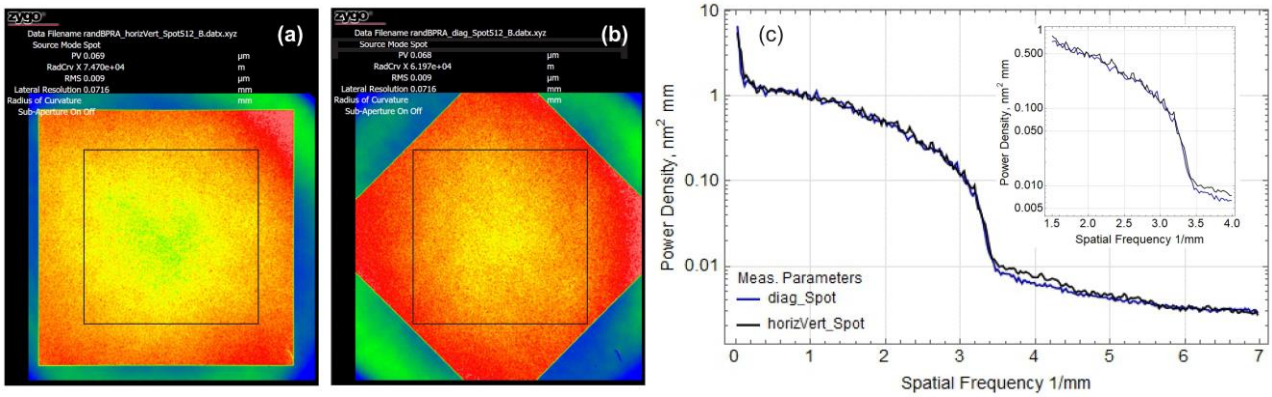

Figure 4. The 15-µm optimal BPRA test sample as measured with 150-mm-diameter aperture Fizeau interferometer (a) in the horizontal and (b) in 45° rotated orientations. The square in the center of plots (a) and (b) depicts the size of the mask used for calculation of the corresponding PSD distributions in plot (c). The measurements were performed in the Spot source mode with the zoom factor of approximately ×2; the effective pixel size is about 72 µm.

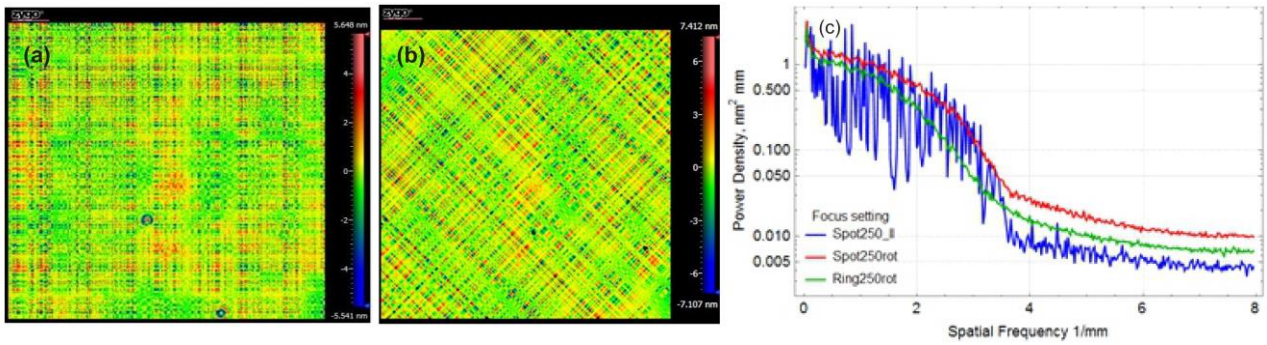

Figure 5. The 15-µm URA BPRA test sample as measured with 150-mm-diameter aperture Fizeau interferometer (a) in the horizontal and (b) in the rotated orientations. (c) The PSD spectra of the 15-µm URA BPRA test sample, corresponding to the sample pattern oriented parallel to the detector (the blue line) and rotated by 45° (the red line) as measured with the interferometer (the same as in Fig. 3) in the Spot source mode; and (the green line) in the Ring source mode with the sample rotated by 45° (for the detailed description of these measurements, see Ref. [4]).

Unlike the interferometric measurements with the URA BPRA test sample measurements (Fig. 5), the PSD distributions of the optimal highly randomized BPRA sample are practically independent of the sample orientation. The isotropy of the optimal BPRA sample depicted in Fig. 4 enables high-confidence measurements of the 2D MTF of Fizeau interferometers (Sec. 6). This is principally important for usage of the measured 2D MTF for sub-resolution reconstruction of 2D data from the interferometers, analogous to the 1D surface slope data reconstruction demonstrated in Ref. [23]. The work on 2D data reconstruction is in progress.

Note that rotation of the 15-µm URA BPRA test sample improves the 1D PSD spectra evaluated for the sample directions along the rows and column of pixels of the instrument's charge-coupled device (CCD) detector. The inherent anisotropy of the rotated URA BPRA pattern is still replicated in the anisotropy of the 2D PSD spectrum.

6. CHARACTERIZATION OF 150-mm-DIAMETER APERTURE FIZEAU INTERFEROMETER IN THE 'SPOT' AND 'RING' MODES OF LASER LIGHT SOURCE

In interferometric measurements of optical surface form, the high spatial coherence of a conventional laser point light source ("spot mode") can lead to errors caused by stray light associated with the optical surfaces used in the metrology system, and imperfections such as dust on the surfaces. Modern interferometers offer ways to reduce coherent noise by reducing the spatial coherence of the light source. This can be done by increasing the size of the light source, e.g. by illuminating a rotating ground glass screen with a slightly defocused laser beam. Some interferometers use a ring light source, which eliminates the fringe localization effects seen in interferometers with extended light sources [22].

Our measurements with the developed highly-randomized BPRA sample have brought out some important peculiarities of the interferometric measurements in the 'Spot' and 'Ring' modes of laser light source when using a zoom factor of larger than ×1.

First, the effective spatial resolution of the measurements appeared to be significantly lower than one would expect based just on the value of the corresponding effective pixel size. This conclusion is illustrated with Fig. 6, where we reproduce the 1D PSD distributions of the 15-μm highly-randomized BPRA test sample as measured with 150-mm-diameter aperture Fizeau interferometer in (a) 'Spot' and (b) 'Ring' modes of laser light source and at two settings of the zoom factor of approximately ×2 and ×3.

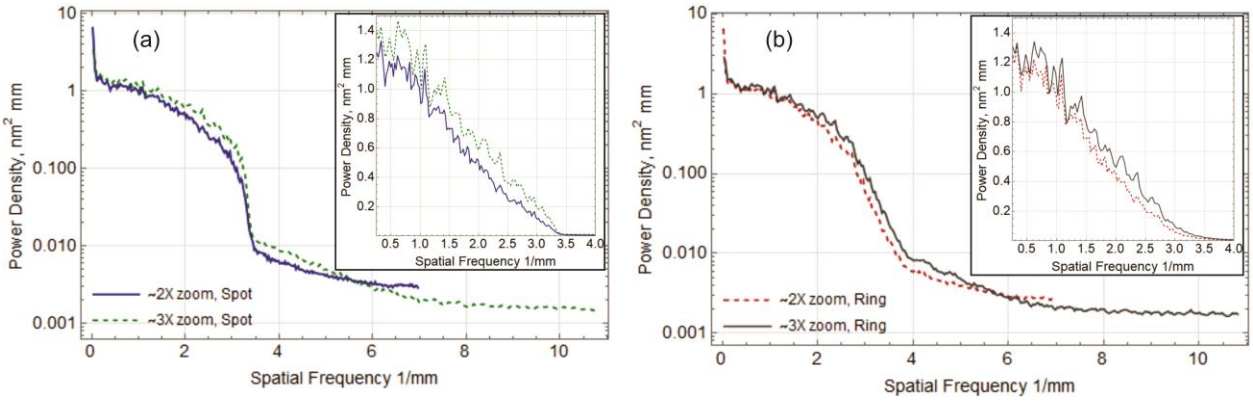

Figure 6. 1D PSD distributions of the 15-μm highly-randomized BPRA test sample as measured with 150-mm-diameter aperture Fizeau interferometer (a) in the 'Spot' and (b) in the 'Ring' modes of laser light source. The measurements were performed at two settings of the zoom of approximately ×2 and ×3; the corresponding effective pixel sizes are 71.6 μm and 46.2 μm.

The applied zoom settings ×2 and ×3 correspond to the effective pixel sizes of 71.6 μm and 46.2 μm, respectively. However, the high spatial frequency cut-off of the PSD distributions in Fig. 6 is at approximately 3.5 mm^{-1} and almost independent on the zoom setting. Assuming that the spatial resolution is determined solely by the interferometer's effective pixel size, the experimentally observed resolution corresponds to a pixel size of about 140 μm. This is approximately the effective pixel size of the interferometer without zoom (the zoom factor is equal to 1) that is ≈160 μm.

Second, the interferometer provides accurate measurements of the surface height topology only up to the spatial frequencies of about 1.5 mm^{-1} corresponding to the surface features with the spatial period of about 0.7 mm. This is clearly seen in the insets to the plots in Fig. 6, where the PSD spectra are shown in a linear scale.

7. CONCLUSIONS AND DISCUSSION

Continuing our work on the project devoted to the development of an efficient and trustworthy method for experimental characterization of different types of metrology tools, we have designed, fabricated, and tested highly-randomized 2D BPRA test samples optimized for the high-accuracy MTF calibration of optical interferometric microscopes and Fizeau interferometers. The optimal BPRA samples have isotropic inherent 2D PSDs with minimal possible variation evaluated over different subareas of the total array when cropped by a factor of 2 to 3.

We have experimentally demonstrated the high level of isotropy of the new BPRA samples, vital for high-confidence measurements of the 2D MTF of metrology instruments. In particular, the 15-μm highly-randomized BPRA sample provides high-accuracy data on the 2D MTF of the Fizeau interferometer in use.

The possibility to measure with high accuracy the 2D MTF is principally important for sub-resolution 2D data reconstruction, analogous to the 1D data reconstruction demonstrated in our recent publication [23]. Development of the required 2D reconstruction (deconvolution) algorithm and dedicated software will allow a significant increase of the resultant lateral resolution of the wide spectrum of the metrology tools just by reprocessing the data based on the accurately measured instrument's MTF. For example, based on the results of characterization of the present Fizeau interferometer discussed in this report (Fig. 6), we can expect an increase of the high spatial frequency limit for the trustful measurements from 1.5 mm^{-1} to approximately 3 mm^{-1}. The work on 2D data reconstruction is in progress.

ACKNOWLEDGEMENTS

The authors are grateful to Timothy Hall, Jeffrey Marron, and Kathy Sharpless of NIST for providing very valuable suggestions to improve the manuscript. This work was partially supported by the U.S. Department of Energy Office of Science, Office of Basic Energy Sciences, and Small Business Technology Transfer programs under Award Numbers DE-SC0011352. Research at the Advanced Light Source and the Molecular Foundry at Lawrence Berkeley National Laboratory is supported by the Office of Science, Office of Basic Energy Sciences, and Material Science Division of the U.S. Department of Energy under Contract No. DE-AC02-05CH11231.

DISCLAIMER

REFERENCES

[1] Molecular Foundry, website: https://foundry.lbl.gov/.

[2] Yashchuk, V. V., Artemiev, N. A., Lacey, I., McKinney, W. R., and Padmore, H. A., "Advanced environmental control as a key component in the development of ultra-high accuracy ex situ metrology for x-ray optics," Opt. Eng. 54(10), 104104 (2015); doi: 10.1117/1.OE.54.10.104104.

[3] Yashchuk, V. V., Anderson, E. H., Barber, S. K., Bouet, N., Cambie, R., Conley, R., McKinney, W. R., Takacs, P. Z., Voronov, D. L., "Calibration of the modulation transfer function of surface profilometers with binary pseudo-random test standards: expanding the application range to Fizeau interferometers and electron microscopes," Opt. Eng. 50(9), 093604 (2011); doi: 10.1117/1.3622485.

[4] Yashchuk, V. V., Babin, S., Cabrini, S., Griesmann, U., Lacey, I., Munechika, K., Pina-Hernandez, C., and Wang, Q., "Characterization and operation optimization of large field-of-view optical interferometers using binary pseudorandom array test standard," Proc. SPIE 10749, 107490R (2018); doi: 10.1117/12.2322011.

[5] Fenimore, E. E. and Cannon, T. M., "Coded aperture imaging with uniformly redundant arrays," Appl. Opt. 17(3), 337–347 (1978); doi: 10.1364/AO.17.000337.

[6] Caroli, E., Stephen, J. B., Di Cocco, G., Natalucci, L., and Spizzichino, A., "Coded aperture imaging in x- and gamma-ray astronomy," Space Sci. Rev. 45, 349–403 (1987); doi: 10.1007/BF00171998.

[7] Barakat, R., "Determination of the Optical Transfer Function Directly from the Edge Spread Function," J. Opt. Soc. Am. 55, 1217-1221 (1965); https://doi.org/10.1364/JOSA.55.001217.

[8] Tatian, B., "Method for Obtaining the Transfer Function from the Edge Response Function," J. Opt. Soc. Am. 55, 1014-1019 (1965); https://doi.org/10.1364/JOSA.55.001014.

[9] Creath, K., "Calibration of numerical aperture effects in interferometric microscope objectives," Appl. Opt. 28 (15), 3333-3338 (1989); doi: 10.1364/AO.28.003333.

[10] Takacs, P. Z., Li, M. X., Furenlid, K., and Church, E. L., "Step-height standard for surface-profiler calibration," Proc. SPIE 1995, 235–244. (1993); https://doi.org/10.1117/12.162661.

[11] Harasaki, A. and Wyant, J.C., "Fringe modulation skewing effect in white-light vertical scanning interferometry," Appl. Opt. 39, 2101-2106 (2000); https://doi.org/10.1364/AO.39.002101.

[12] Boreman, G.D. and Yang, S., "Modulation Transfer Function Measurement Using Three- and Four-bar Targets," Appl. Opt. 34, 8050-8052 (1995); 10.1364/AO.34.008050.

[13] Marchywka, M. and Socker, D. G., "Modulation transfer function measurement technique for small-pixel detectors," Appl. Opt. 31(34), 7198-7213 (1992); ttps://doi.org/10.1364/AO.31.007198.
[14] Nijhawan, O. P., Datta, P. K., and Bhushan, J., "On the measurement of MTF using periodic patterns of rectangular and triangular wave-forms," Nouv. Rev. Opt. 6(1), 33-36 (1975); https://iopscience.iop.org/article/10.1088/0335-7368/6/1/304.
[15] Rhee, H. G., Vorburger, T. V., Lee, J.W., and Fu, J., "Discrepancies between roughness measurementsobtained with phase-shifting and white-light interferometry," Appl. Opt. 44(28), 5919-5927 (2005); https://doi.org/10.1364/AO.44.005919.
[16] Wolfram Research, Inc., Wolfram Mathematica Tutorial Collection: Random Number Generation pp. 1-44 (2008); https://library.wolfram.com/infocenter/Books/8507/RandomNumberGeneration.pdf (last access: June, 2020).
[17] "EViews 8 user's guide," Volumes I and II, Quantitative Micro Software; www.eviews.com (last access: June, 2020).
[18] Tyurina, A. Y., Tyurin, Y. N., and Yashchuk, V. V., "Stochastic Analysis of Surface Metrology," Opt. Eng. 58 (08), 084101 (2019); doi:10.1117/1.OE.58.8.084101.
[19] Hart, J. D., Terashima, Y., Uchida, A., Baumgartner, G. B., Murphy, T. E., and Roy, R., "Recommendations and illustrations for the evaluation of photonic random number generators," APL Photonics 2, 090901/1-23 (2017); https://doi.org/10.1063/1.5000056.
[20] Herrero-Collantes, M. and Garcia-Escartin, J. C., "Quantum random number generators," Rev. Mod. Phys. 89(1), (2017); https://doi.org/10.1103/RevModPhys.89.015004.
[21] Inubushi, M., Yoshimura, K., Arai, K., and Davis, P., "Physical random bit generators and their reliability: focusing on chaotic laser systems," Nonlinear Theory and Its Applications, IEICE 6(2), 133–143 (2015); doi: 10.1587/nolta.6.133.
[22] Küchel, M., "Spatial Coherence in Interferometry: Zygo's new method to reduce intrinsic noise in interferometers," Zygo Corporation Library, 2004; www.zygo.com (last access: June, 2020).
[23] Yashchuk, V. V., Lacey, I., Arnold, T., Paetzelt, H., Rochester, S., Siewert, F., and Takacs, P. Z., "Investigation on lateral resolution of surface slope profilers," Proc. SPIE 11109, 111090M (2019); doi: 10.1117/12.2539527.